Development 140, 395-404 (2013) doi:10.1242/dev.087940

Quantitative analysis of polarity in 3D reveals local cell coordination in the embryonic mouse heart

Jean-François Le Garrec[1,2,*], Chiara V. Ragni[1,2], Sorin Pop[3,4], Alexandre Dufour[3,4], Jean-Christophe Olivo-Marin[3,4], Margaret E. Buckingham[1,2] and Sigolène M. Meilhac[1,2,*]

SUMMARY

Anisotropies that underlie organ morphogenesis have been quantified in 2D, taking advantage of a reference axis. However, morphogenesis is a 3D process and it remains a challenge to analyze cell polarities in 3D. Here, we have designed a novel procedure that integrates multidisciplinary tools, including image segmentation, statistical analyses, axial clustering and correlation analysis. The result is a sensitive and unbiased assessment of the significant alignment of cell orientations in 3D, compared with a random axial distribution. Taking the mouse heart as a model, we validate the procedure at the fetal stage, when cardiomyocytes are known to be aligned. At the embryonic stage, our study reveals that ventricular cells are already coordinated locally. The centrosome-nucleus axes and the cell division axes are biased in a plane parallel to the outer surface of the heart, with a minor transmural component. We show further alignment of these axes locally in the plane of the heart surface. Our method is generally applicable to other sets of vectors or axes in 3D tissues to map the regions where they show significant alignment.

KEY WORDS: Cell polarity, Mouse heart morphogenesis, Clustering, Axial correlation, Directional statistics

INTRODUCTION

Most cells, in multicellular or unicellular organisms, are polarized. Cell polarities and orientations, i.e. vectorial and axial information, play a major role in the morphogenesis of the embryo, by influencing cell fate diversification, tissue architecture and the shape of organs (Morin and Bellaïche, 2011; Lecuit and Lenne, 2007). In the adult heart, the myocardium has a myofiber architecture that corresponds to the alignment of cardiomyocytes and is essential for the efficient contraction of the heart (Jouk et al., 2000). This is associated with an elongation of cells, which arises progressively during development (Risebro et al., 2009). In the embryonic heart, no such anisotropy of the cellular architecture has been reported, although growth of the myocardium is oriented (Meilhac et al., 2004a) and planar cell polarity (PCP) pathways are required for heart morphogenesis (Henderson and Chaudhry, 2011).

Cell polarity involves an asymmetric distribution of components of polarity signaling pathways, usually described in two modes: planar and apico-basal polarity (Zallen, 2007). In the heart, the myocardium is not an epithelium. However, growth of the myocardium can also be described in two modes, referred to as planar and transmural (Meilhac et al., 2003). The position of organelles is another indicator of cell polarity; for example, the centrosome (Bornens, 2008), which is involved in the organization of the Golgi, the primary cilium and the microtubule cytoskeleton, may polarize several cellular processes (Badano et al., 2005). The alignment of animal hairs exemplifies the fact that polarities may be coordinated between neighboring cells. This is already prefigured in embryonic tissues, as in the fly pupal wing, in which the polarized localization of components of the PCP pathway prefigures the alignment of the wing hairs (Strutt, 2001; Wu and Mlodzik, 2009). This planar polarity is global and affects all cells in the disc. In other instances, such as during the growth of the limb bud, cell polarity or orientation of cell division is more local, and varies between regions within the tissue (Boehm et al., 2010; Gros et al., 2010). Elongation of the anterior-posterior axis of the fish embryo involves oriented behavior, such as cell division (Gong et al., 2004), and is associated with a polarized localization of the centrosome (Sepich et al., 2011). These polarities are dynamic: they are not detectable at midgastrulation stages and are initiated only by late gastrulation. Understanding how cell polarities are coordinated requires quantitative analysis of the spatial distribution of polarity markers.

Until now, studies on cell polarity or on oriented cell behavior have been conducted in simple epithelia with a planar geometry (Baena-López et al., 2005; Blankenship et al., 2006; Goodrich and Strutt, 2011), or in tissues that have clear reference axes, such as an axis or plane of symmetry (Concha and Adams, 1998). In these models, cell orientations can be described by a single angle and their alignment can be analyzed in 2D with standard circular statistical tests. However, in other tissues, which have a less organized cell architecture and a more complex geometry, it is not possible to perform the analysis in 2D or to find a simple reference axis. This is the case for the embryonic mouse heart, which is a looped tube (Harvey, 2002). Moreover, the variance in directions is high, because the third dimension introduces an additional degree of freedom and because cell behavior in the mouse is not stereotyped. For such studies in 3D, development of appropriate statistical tools is required.

Advances in statistics of 3D axial distributions have been made in disciplines other than biology. Mathematical tools are available to assess the anisotropy of such distributions and estimate the degree of axial coordination based on the eigenvalue method (Mardia and Jupp, 2000). A classical problem in computer graphics, when aiming to reproduce the movement of people in

[1]Institut Pasteur, Unit of Molecular Genetics of Development, Department of Developmental Biology, F-75015 Paris, France. [2]CNRS, URA2578, F-75015 Paris, France. [3]Institut Pasteur, Unit of Quantitative Image Analysis, Department of Cell Biology and Infection, F-75015 Paris, France. [4]CNRS, URA2582, F-75015 Paris, France.

*Authors for correspondence (jean-francois.le-garrec@pasteur.fr; sigolene.meilhac@inserm.fr)

Accepted 22 October 2012

animated cartoons, is to simplify a high-resolution complex 3D shape into a small number of surfaces that approximate nearly co-planar mesh vertices. This problem, which was solved by a K-means clustering algorithm (Cohen-Steiner et al., 2004), is formally equivalent to our search for regions where cell orientations tend to be aligned. In geological sciences, tools for the analysis of 3D orientation data are widely used to describe sedimentary facies or strain histories with fabric shape diagrams. It has been shown that the size of the sampling is crucial for defining confidence regions, in which the sample represents the true fabric shape (Ringrose and Benn, 1997). In statistical physics, the spatial correlation function is routinely used to estimate the dependency relationships of observations across space. This is relevant to estimate the range over which a cell polarity is aligned with that of its neighbors. Although quantitative analysis of cell polarities on a tissue scale in 3D is a current issue in developmental biology, biology lags behind other disciplines in the availability of tools to analyze the coordination of polarities.

Building on these multidisciplinary principles, we present here a novel methodology for the analysis of tissue polarity in 3D. This is a generalization of the clustering algorithm, in which we have introduced a bootstrap method to dispense with any arbitrary parameter, as well as statistical constraints adapted to weak correlations and curved geometries. We took the developing mouse heart as a model and examined the orientation of several markers of tissue anisotropy. Image analysis tools were used to automatically extract the 3D axial information from confocal scans. Our methodology demonstrates that neighboring cells are already locally coordinated in the embryonic myocardium.

MATERIALS AND METHODS

Immunostaining of isolated hearts

Hearts were dissected from embryos at embryonic day (E) 8.5 or E13.5 of the R26-mT/mG (Muzumdar et al., 2007) mouse line and fixed in 0.5% paraformaldehyde overnight at 4°C. To preserve heart geometry, fluorescent immunostaining was performed as a whole mount, with an anti-Pcnt (BD Biosciences 611814 or Covance PRB-432C) primary antibody to label centrosomes, anti-DsRed (Clontech 632496) to label membranes, anti-AurkB to label the cytoplasmic bridge that links sister cells (BD Biosciences 611082) and Hoechst counterstaining to label nuclei. Samples were rinsed with PBX (PBS + 0.1% Triton), permeabilized in 0.75% Triton and blocked in 10% inactivated goat serum and 0.5% Triton. Before the blocking, aldehydes were quenched in 2.6 mg/ml NH_4Cl. All experiments with animals were conducted in accordance with the regulations of the French Ministry of Agriculture.

Orientation of clonal growth

Clones of β-galactosidase positive cells were taken from a collection generated previously from the α_c-*actin*$^{nlaacZ1.1/+}$ mouse line (Meilhac et al., 2004b). Clones were selected for their localization in the posterior view of the looped E8.5 heart (Fig. 3A) and mapped onto a reference heart contour as previously described (Meilhac et al., 2004a).

Image acquisition and segmentation

Hearts were mounted in Fluoromount G between coverslips, using a spacer. Multi-channel 16-bit images were acquired with a Leica SP5 inverted confocal microscope, and a 40×/1.25 oil immersion objective. Z-stacks over 30 μm were scanned every 1 μm. The size of a scan is 1024×1024×30 voxels, with a resolution of 0.379×0.379×1 μm.

The nuclei were segmented as previously described (Pop et al., 2011b). Briefly, the nuclear channel was filtered and, to improve the separation of adjacent nuclei, the membrane channel was processed through an anisotropic diffusion filter (Pop et al., 2011a), and subtracted from the filtered nuclear channel. The final segmentation was achieved by a 3D active mesh method initiated from each pre-detected nucleus (Dufour et al., 2011).

The centrosomes were segmented with the wavelet-based spot detector (Olivo-Marin, 2002) using two scales and a threshold between 10 and 20.

The cells at E8.5 were segmented by the 3D active mesh method initialized from the segmented nuclei and applied to the filtered membrane channel (S.P., A.D., J.-F.L.G., C.V.R., C. Cimper, S.M.M. and J.-C.O.-M., unpublished). At E13.5, a watershed algorithm was used to segment the filtered membrane channel. The axis of cell elongation was defined as the first eigenvector V_1 of the segmented cell envelope.

To pair the centrosome and nucleus of the same cell, the nearest nucleus was searched in the vicinity of a centrosome (supplementary material Fig. S2D). We measured that the average distance between the centroid of a nucleus and that of its related centrosome is 3.9±1.1 μm (n=80 cells), with a maximum distance of 7.2 μm. Consequently, an error of one voxel in the location of a centroid may lead to a 6 degree error in the axis direction [arctangent(0.4/3.9), with a voxel size of 0.4 μm]. Therefore, we limited our automatic pairing procedure to favor the quality of the data over the quantity, by eliminating incorrect segmentations or mitotic cells. The centrosome-nucleus pair was retained only if (1) both centroids were inside the same segmented cell, (2) the nucleus size was inside the range (median size ± standard deviation), (3) the nucleus was paired to a single centrosome and (4) the centrosome-nucleus distance was less than 7 μm. About half the total number of cells were retained for further analysis of their centrosome-nucleus axes (typically about 200-400, supplementary material Fig. S2E). From the paired centroids of the nucleus and the centrosome, we calculated the axis of cell polarity as the coordinates of a vector of unit length (Vx, Vy, Vz). Hence, the axial data consist of a set of six coordinates per cell (supplementary material Fig. S2D,E) corresponding to the centrosome position and the axis of cell polarity.

To detect orientation of cell division in E8.5 embryos, the cytoplasmic bridges were segmented by thresholding after anisotropic filtering and enhancement. Sister cells were identified by a scoring function taking into account both the distance from the bridge extremity and the direction of the bridge (S.P., A.D., J.-F.L.G., C.V.R., C. Cimper, S.M.M. and J.-C.O.-M., unpublished). In E13.5 embryos, where the thicker tissue is less amenable to imaging and automatic bridge segmentation, sister cells were identified manually. Both procedures ended with the calculation of the axis of cell division, joining the paired centroids of the nuclei of the two sister cells.

All the plug-ins used here are related to the ICY software and are open-source (de Chaumont et al., 2012).

K-means clustering algorithm

The MATLAB code of the clustering algorithm is given in supplementary material Appendix S1.

Bootstrap

For each region size (from 1 to N), 10,000 random sets of axes were generated by randomly drawing, with replacement, axes from the original data set. This was carried out by permuting randomly the rank of the triplets $V_xV_yV_z$ (direction) so that they are associated with a new triplet XYZ (position). This method was found to be more stringent than permuting separately V_x, V_y and V_z, as the planar bias means that there is a correlation between the three coordinates of the direction vector. The random sets were sorted in increasing order of their eigenvalue E_1, and we determined the threshold eigenvalue $E_{1(5\%)}$ above which the best 5% of sets are to be found for a region of a given size (supplementary material Fig. S1D). Regions of different sizes are thus compared by the ratio $E_1/E_{1(5\%)}$, indicating how they deviate from the threshold above which there is less than 5% probability that the axial coordination is due to chance. The degree of axial coordination per region ($E_1/E_{1(5\%)}$) was better for higher K-values, which tended to produce smaller regions (supplementary material Fig. S1E). The significance of the axial coordination in the best oriented regions was confirmed by a statistical test.

Minimum region size

In the case of a girdle distribution ($E_1 \approx E_2 \gg E_3$), it is necessary to take into account the sampling size. It has been shown that too small a sample may

lead to apparent swapping between the V_1 and V_2 eigenvectors, as they are distinguished by their relative length, which may vary, and not by their direction. This implies that the preferred orientation of the sample may appear different from that of the original population. Ringrose and Benn (Ringrose and Benn, 1997) have shown that the swapping risk is reduced to an acceptable level if a minimum size of the sample is set according to its elongation $E=1-(E_2/E_1)$. For moderately elongated distributions ($E\approx0.3$), as is the case for our E8.5 samples, more than 50 points per region are required. For more elongated distributions ($E>0.4$), such as in our E13.5 samples or synthetic data sets, the minimum region size may be lowered to 30 points.

Statistical tests

The Bingham test formalizes the intuitive idea that isotropy may be rejected if the three eigenvalues are far from N/3. It rejects spherical uniformity for large values of the statistic $B=(15/2)\times N\times\{\text{trace}(SM^2)-1/3\}$, where N is the size of the sample and SM the following scatter matrix:

$$\begin{pmatrix} \Sigma V_x^2 & \Sigma V_x V_y & \Sigma V_x V_z \\ \Sigma V_y V_x & \Sigma V_y^2 & \Sigma V_y V_z \\ \Sigma V_z V_x & \Sigma V_z V_y & \Sigma V_z^2 \end{pmatrix},$$

where V_x, V_y and V_z are the three vector coordinates of each cell axis, and Σ is the sum over the sample of axes. The threshold value is that of a chi-square distribution with 5 degrees of freedom. Anderson-Stephens' test is based on the comparison of the eigenvalues to one another. For large values of E_1, uniformity is rejected in favor of a bipolar distribution, while for small values of E_3 it is rejected in favor of a girdle distribution. For the threshold values, see Anderson and Stephens (Anderson and Stephens, 1972).

Giné's test, which is not based on the eigenvalues but on the angles between the axes, rejects spherical uniformity for large values of the statistic $G=N/2-\text{SumSin}\times\{1/(N\times\Gamma(3/2)^2\}$, where SumSin is the sum of the sine of all the angles made by pairs of axes in the sample and Γ is the gamma function (Mardia and Jupp, 2000).

The Rayleigh circular test rejects uniformity for large values of the Rayleigh number (R), which is the length of the mean vector. For axial data, as distinct from vectorial data, the angles to the reference axis are doubled before calculating R (Mardia and Jupp, 2000). This 2D test was applied to regions of interest by projecting all the original 3D axes on the same local plane, chosen as the tangent to the surface point closest to the center of the region.

Axial correlation

We calculated the axial correlation as the average of the scalar product $\langle|V_i\cdot V_j|\rangle$, computed over all (i,j) pairs of planar axes V separated by a distance divided equally into 40 bins with a width of 10 μm. For each of the seven scans, 100 random samples were obtained by associating with each axis position of the scan a random orientation in the local tangent plane. These 700 random samples were averaged (with a weighting proportional to the number of axes in each scan) to derive their correlation as a function of distance. The standard deviation of the correlation in each of the 40 bins was calculated to obtain the 95% confidence interval (average±1.96×s.d.).

Correlation maps of the extent of axial coordination were produced by calculating the average axial correlation curve for all axes situated in 100×100×30 μm boxes, shifted every 10 μm along both the *x* and *y* axes. The extent of axial coordination was taken as the distance (divided equally into 20 bins with a width of 20 μm) where this curve intersects a threshold line. Owing to the small sample size, a threshold of 0.62 (determined empirically) was retained for all maps. Note that the extent of axial correlation depends on the threshold and is a relative measure.

Modeling patterns of cell orientation

The positions (XYZ) of the axes were taken from a real data set of 250 axes. The 3D orientations of the axes ($V_xV_yV_z$) were allocated randomly in three steps. Axes were calculated according to the chosen pattern (parallel or concentric). A rotation vector was drawn randomly for each axis from a uniform distribution over the sphere. Angles of rotation around this vector were drawn randomly for each axis from a normal distribution (mean=0; standard deviation=0.1 π). This procedure was implemented with the MATLAB RandStream method, using the Mersenne twister random generator.

RESULTS

3D statistical tests show the planar anisotropy of cell axes

We have designed a method for analyzing tissue anisotropy in 3D, which we first validated in a tissue that is known to be anisotropic. The fetal heart provides such a model, as it was reported that the myocardium has an anisotropic architecture, including elongated cells with concordant elongation of the sarcomeres (Risebro et al., 2009). Thus, we monitored the elongation of cells in E13.5 hearts (Fig. 1A). 3D images in the ventricle were analyzed with segmentation algorithms to extract automatically the axes of cell elongation (Fig. 1A′).

We investigated whether the overall distribution of axes significantly deviates from an isotropic spherical distribution. 3D axial distributions may be represented by three principal directions (eigenvectors V_1, V_2, V_3), and their associated eigenvalues (E_1, E_2, E_3), which are numbered such that $E_1>E_2>E_3$, with $E_3+E_2+E_1=N$, where N is the number of axes in the sample (Mardia and Jupp, 2000). We compared the observed distribution to theoretical models. For an isotropic distribution of axes over the sphere, E_1 is minimal and equals N/3 (Fig. 1B), whereas in an anisotropic bipolar distribution, the average direction of the set of axes is that of the eigenvector V_1 and the concentration of the axes around this average direction is measured by the associated eigenvalue E_1 (Fig. 1B′). We applied three statistical tests of uniformity of axial data to our observations. The Bingham test rejected isotropy, as did Giné's test ($P<0.001$, $n=1588$). The complementary test of Anderson and Stephens, which is more informative as it can distinguish between non-isotropic distributions (Fig. 1B′,B″), rejected isotropy in favor of a bipolar, but not a girdle, distribution (Fig. 1C). This means that the axes of cells in the fetal heart follow a preferential direction indicated by the eigenvector V_1 of the sample, which had a low component along the transmural axis of the heart.

Such planar bias can be confirmed by measuring the angles between the axes of cells and the transmural axis: the observed distribution differed significantly from a random distribution and showed a higher concentration around 90° (Fig. 1D). With this approach, we can thus correctly detect the planar bias of cell axes corresponding to the myofiber architecture, which is parallel to the surface in this ventricular region of the fetal heart.

K-means clustering reveals regions of significant axial coordination

Within the plane where they are biased, we analyzed cell orientations in order to understand whether all cells follow the same preferential direction. We investigated whether there were regions where the axes were significantly aligned between neighboring cells. By partitioning the tissue into a regular grid, a map of local average directions can be drawn, which indicates qualitatively the orientation of anisotropy (Fig. 2A). However, such a map does not indicate whether there is indeed axial coordination with statistical significance.

To avoid arbitrary partitions of the tissue into regular regions with no biological significance, or into preconceived regions, such as the regions defined by anatomical or molecular landmarks, we

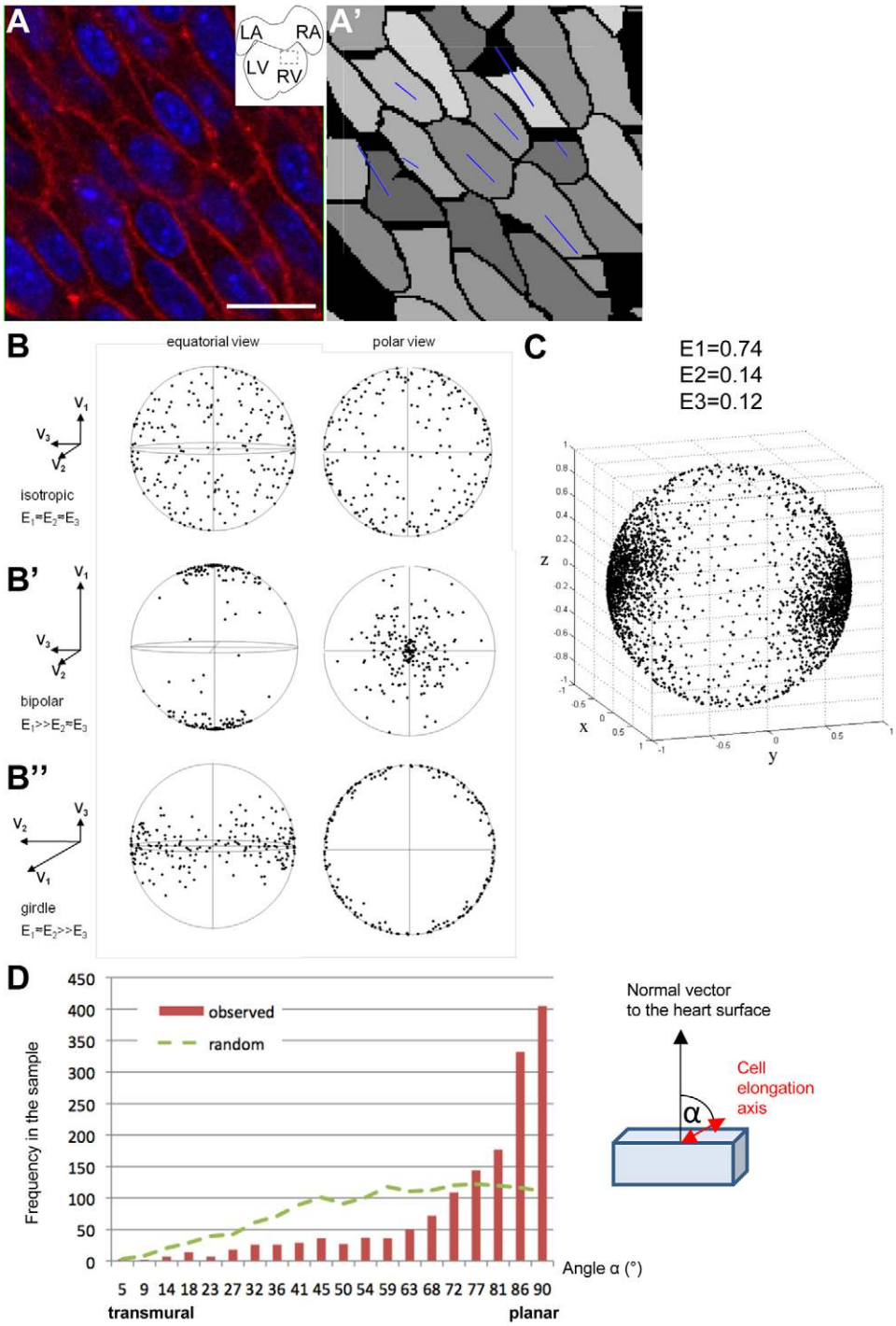

Fig. 1. The axes of cell elongation in the fetal heart show a planar orientation. (**A**) Example image of myocardial cells, with labeled nuclei (blue) and membranes (red). The inset indicates the frame of the dataset in the E13.5 heart, viewed dorsally. Scale bar: 10 μm. (**A′**) After segmentation, the axes of cell elongation (2D projection in blue) are extracted. (**B-B″**) Models of axial distributions. The sphere represents the 3D space, from an equatorial (left) or polar (right) view, and the dots indicate the extremities of axes on the surface of the sphere. In an isotropic distribution (B), the extremities of axes have no pattern, and the average direction is decomposed in eigenvectors (V1, V2, V3) of equal length or eigenvalues (E1, E2, E3). By contrast, two types of anisotropic distributions may be distinguished, with concentrations of the extremities of axes at the poles (B′) or in the equatorial plane (B″). (**C**) The observed distribution of the axes of cell elongation is significantly non-isotropic and bipolar (Anderson-Stephens' statistical test, $P<0.01$, $n=1588$ axes). (**D**) The observed distribution (red) of the angles between the axis of cell elongation and the vector normal to the heart surface significantly deviates from a random spherical distribution (green dotted line) and indicates a planar bias (Student's *t*-test, $P<0.001$, $n=1588$). LA, left atrium; LV, left ventricle; RA, right atrium; RV, right ventricle.

designed a fast search algorithm identifying objectively the regions with the best axial coordination between cells. The algorithm was adapted from a K-means clustering method initially designed for computer graphics (Cohen-Steiner et al., 2004). It is based on a single input parameter that is the number, K, of regions in the partition. The algorithm starts from K seeds chosen randomly among the data points, and grows regions iteratively around the seeds by allocating to each region neighboring cells with more similar orientations (supplementary material Fig. S1B). The algorithm results in an optimal partition, as the sum of individual deviations of axes from the average direction of their region is minimized.

To dispense with the arbitrary parameter K, we developed a procedure to select regions from multiple runs of the algorithm with varying K values. A bootstrap method (Efron and Tibshirani, 1993) was used to rate the regions based on their degree of axial coordination independently of their size. Regions were pre-selected according to their associated eigenvalue E1 (above the 5% threshold of the bootstrap method) and to their size (above a threshold as in Ringrose and Benn, 1997). Finally, to draw the resulting unique map, the best oriented regions were selected in decreasing order of axial coordination, provided that they do not intersect with any of the previously selected regions (supplementary material Fig. S1F).

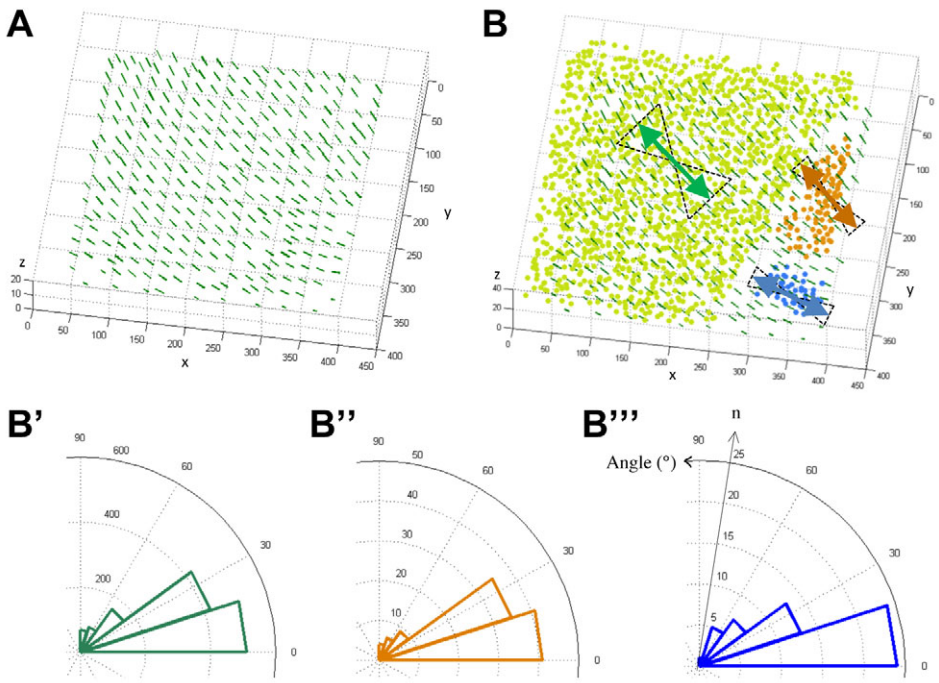

Fig. 2. Map of regions where cells significantly coordinate their axes of elongation. (**A**) Map showing the local average directions of the axes of cells, calculated in 100×100×30 µm boxes (representing about 30 cells) shifted every 20 µm along both the *x* and *y* axes. Each green bar corresponds to the direction of the eigenvector V_1 of the axes within a box, with a length proportional to its eigenvalue. Thus, when axes are locally more parallel, the green bar is longer. (**B**) Map of the regions with significant axial coordination. The average directions per region (double-headed arrows) and the corresponding standard deviations (dotted lines) are shown. The three regions are color coded on the map of the local average directions per box (green bars). (**B′-B‴**) Rose diagrams (16 bins) of the distribution of angles for each of the three regions illustrate the concentration of cell axes around the average direction per region (significant Giné's test, $P<0.01$, $n=1246$, 95 and 50, respectively).

The clustering algorithm was applied to the fetal heart. Three significantly oriented regions were identified in the output map (Fig. 2B). With our quantitative approach, we can thus reveal the regional coordination of axes that corresponds to the myofiber architecture of the fetal heart.

Tissue anisotropy in the embryonic heart: coordination of the axes of cell polarity

Whereas the architecture of the fetal myocardium was reported to be anisotropic, this is not the case for the embryonic heart, based on cell elongation and sarcomere orientation (Risebro et al., 2009). However, as growth of the embryonic myocardium is oriented (Meilhac et al., 2004a), we investigated the anisotropy of this tissue, by applying our methodology using another marker. As a marker of cell polarity in the embryonic E8.5 mouse heart, we monitored the position of the centrosome with respect to the nucleus (Fig. 3A). We frequently observed anti-parallel orientations of the centrosome-nucleus vectors in neighboring cells (supplementary material Fig. S2B″, arrows); therefore, we focused on the axial component of centrosome-nucleus polarity. Images were analyzed with segmentation algorithms (supplementary material Fig. S2A-C) to extract automatically the centrosome-nucleus axes, using an automatic pairing procedure of the centrosome and the nucleus of the same cell (supplementary material Fig. S2D). We confirmed the validity of the pairing by visual checks on a sample ($n=160$, 100% correct).

We first investigated the anisotropy of the overall distribution of the axes of cell polarity and show that it follows a girdle distribution (Bingham test $P<0.001$ with $n=1479$ cells pooled from seven embryos, Anderson-Stephens' test $P=0.01$). This means that the axes of cell polarity in the heart lie preferentially in a plane. To characterize the plane, we measured the angles between the axes and the local transmural axes (Fig. 3B): they were significantly more concentrated around 90° compared with a random distribution (Fig. 3C). We conclude that the axes of cell polarity in the embryonic heart tend to lie preferentially in a plane parallel to the outer surface of the heart.

Within the plane where they are biased, the axes of cell polarity could be further coordinated. The following analysis focuses on the planar components of the axes of cell polarity, defined as their projection on the local plane, tangential to the outer surface of the heart at the point of the surface closest to the nucleus under consideration. As the heart surface is curved (Fig. 3B), the planar components still constitute a set of 3D axes. The clustering algorithm was applied to the embryonic heart (supplementary material Fig. S1). Taking one heart as an example, one significantly oriented region was identified (Fig. 3D). Similarly, in other samples ($n=7$) we found regions of significant axial coordination, although the anatomical location of the regions identified was not stereotyped. These results show a significant local coordination of the axes of cell polarity in regions of the embryonic heart.

Validation of the local axial coordination with the correlation function and computer modeling

As regions identified as significantly oriented with this marker are not stereotyped, it may indicate that the local coordination of the centrosome-nucleus axes between cells is weak. To validate and characterize the local coordination between cardiac cells, we used the axial correlation function derived from physics. We pooled data from seven different embryos to assess the range over which the orientations of two cells may vary together. A practical definition for this, referred to as the length of axial correlation, is the distance over which the correlation function significantly deviates from the random level. Considering the cells of the significantly oriented regions, we validated the correlation of their axes, and further calculated that the length of axial correlation is of the order of 110 µm (Fig. 4A). Our observations thus reveal that cardiac cells locally align their axes of cell polarity, and that the range of this coordination is in the order of 10 cells.

The map of local average directions (supplementary material Fig. S1A) for the heart shown in Fig. 3D would also be compatible with a concentric pattern of the axes of cell polarity. To distinguish between parallel and concentric coordination, we modeled the two possibilities. Using the same heart geometry and cell sampling as

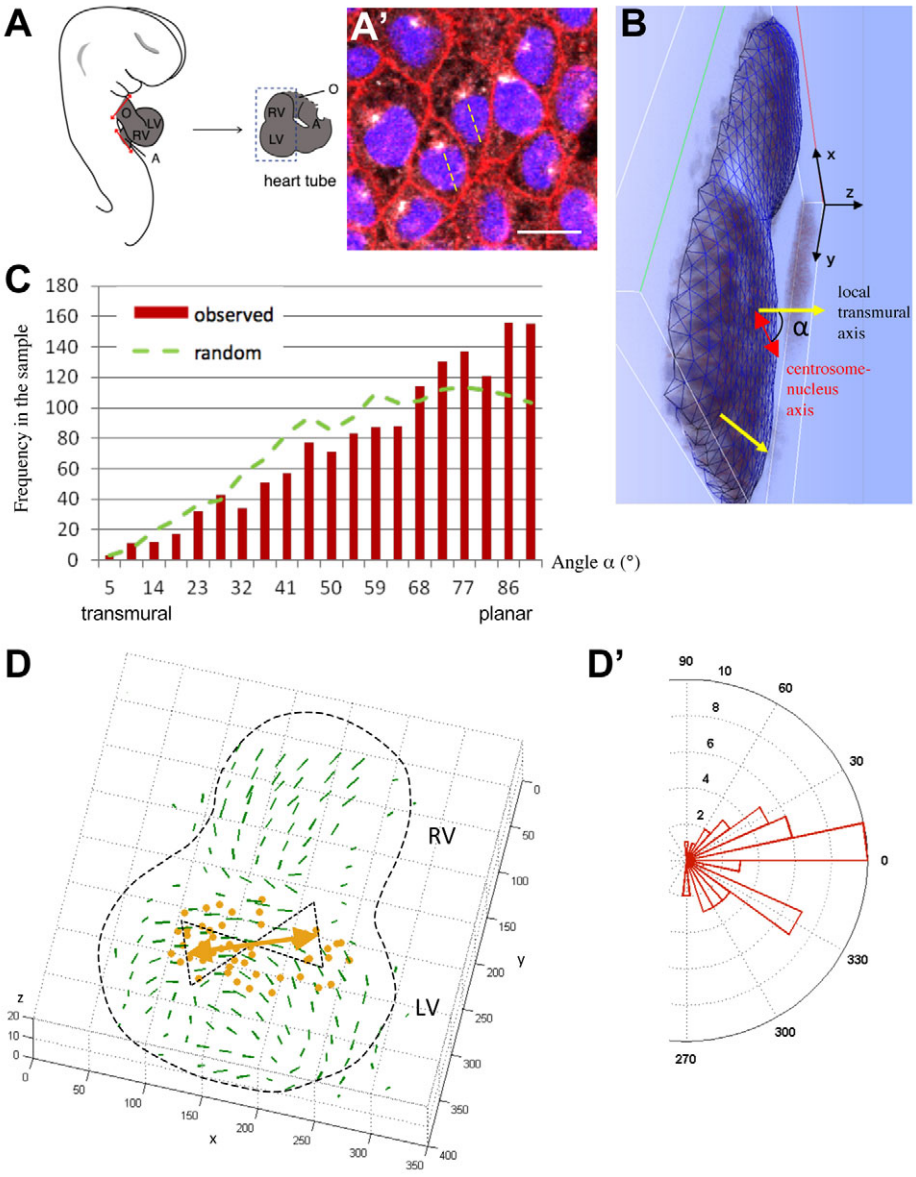

Fig. 3. Local coordination of centrosome-nucleus axes in the embryonic heart. (**A**) For 3D imaging, the embryonic heart was dissected out from the embryo (red double-headed arrows) and scanned in the plane indicated on the right. Using an inverted microscope, the scan is the mirror image of the real sample. (**A′**) Example of an image of myocardial cells, with labeled nuclei (blue), membranes (red) and centrosomes (white). The centrosome-nucleus axes are represented by broken yellow lines. Scale bar: 10 μm. (**B**) 3D mesh showing the outer surface of the heart at E8.5 and the *xyz* axes along which the coordinates were measured. The transmural axis (in yellow) was defined locally for a given nucleus as perpendicular to the outer surface at the closest surface point. (**C**) Distribution of the angles between the centrosome-nucleus axis (red arrow) and the local transmural axis (yellow arrows). The observed distribution was significantly different (Student's *t*-test, $P<0.001$, $n=1479$ cells pooled from seven embryos) from a random spherical distribution and indicates a planar bias. (**D**) Output map of the clustering algorithm, revealing an example of a region (colored dots) with significant axial coordination of the planar components of the axes of cell polarity. The average direction of the region (double-headed arrow) and corresponding s.d. (dotted line) are shown. The green bars indicate the local average directions per box. (**D′**) The rose diagram (16 bins) illustrates the significant concentration of axes around the average direction of the region (Rayleigh circular test, $P=0.001$, $n=50$). A, atria; LV, left ventricle; RV, right ventricle; O, outflow tract.

in the original dataset, we tested the hypothesis that there are three regions of axial coordination (Fig. 4B). Three directions were imposed on cell orientations, taking into account random fluctuations with a standard deviation of 18 degrees, that corresponds to 20% of the maximum noise. Despite this noise, our clustering algorithm correctly identifies the three regions of axial coordination as defined in the model, with a precise determination of the average direction of the regions (Fig. 4B′). The sparse sampling hinders statistical conclusions being drawn about some of the cells, which, as a consequence, are not included in any region. Therefore, the power of the algorithm is to identify a significant subset of axes in the oriented regions. In addition, we have assessed the extent of axial coordination in a correlation map (Fig. 4B″). According to this hypothesis, the expected correlation is higher in the regions of parallel coordination and lower at the boundary between them. In a similar way, we tested the alternative hypothesis: that there are two regions where the axes of cell polarity are concentric (Fig. 4C). Our clustering algorithm identifies a few regions of axial coordination, with concentric average directions (Fig. 4C′). The expected correlation is lower close to the center of the region and higher further away (Fig. 4C″). Therefore, coupling the clustering algorithm to a correlation map makes it possible to distinguish between the two hypotheses. By comparison with the predictions derived from the model, the biological sample was analyzed. No concentric pattern was detected in the correlation map of the observed directions (Fig. 4D), whereas the region of axial coordination identified by the clustering algorithm (Fig. 3D) corresponded to a region of higher correlation. We conclude that our observations in the heart support a model of parallel coordination of cells. These results validate the anisotropy of the embryonic myocardium, with a local coordination of the axes of cell polarity.

Cell division is oriented in the developing heart

To monitor whether cell behavior follows the anisotropy of myocardial architecture, we analyzed the orientation of cell division. Sister cells after mitosis are still connected by a cytoplasmic bridge, which is positive for AurkB (Fig. 5A). From the detection of the bridge, we associated sister cells and extracted the axes of cell division (Fig. 5B). In the fetal heart, we found that

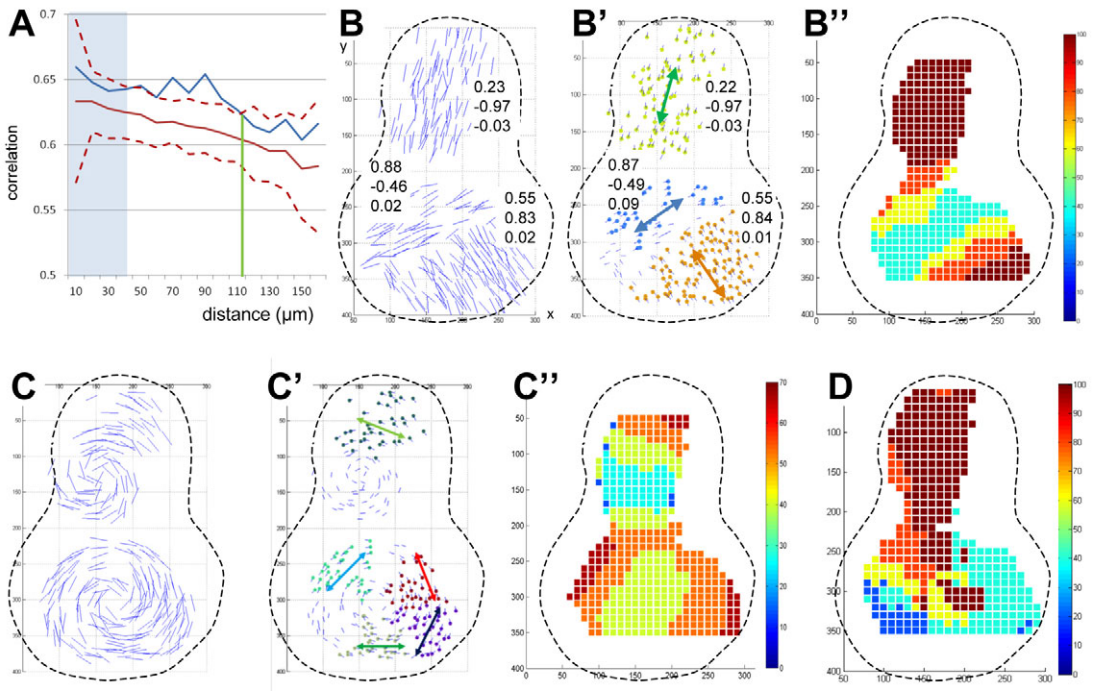

Fig. 4. Validation of the clustering method by measuring correlations and analyzing synthetic data sets. (**A**) Correlation function of the planar components of the centrosome-nucleus axes (n=473) in the significantly oriented regions from seven embryos. The observed distribution (blue) is compared with the average distribution (red line) of random orientations and its 95% confidence interval (red dotted lines). The random correlation is a decreasing function of distance because of the planar bias on a curved surface (more distant axes tend to be less parallel). The observed distribution is above the 95% confidence interval of randomly oriented axes for distances shorter than 110 μm (vertical green line). A lower sampling (the average number of axes per bin is less than 4) at shorter distances causes the observed distribution to lie within the random confidence interval (pale blue shading). (**B**) Synthetic data set of the embryonic heart analyzed in Fig. 3D, produced by arbitrarily defining three regions with axial coordination around the specific average directions indicated (*xyz* coordinates). Noise was applied to the average axis of each cell. (**B′**) Result of the clustering algorithm showing the regions with significant axial coordination. (**B″**) Correlation map of the extent of axial coordination (color coded) per box. (**C**) Synthetic data set produced by arbitrarily defining two regions with a concentric pattern of axes. The same noise was used to calculate the axis of each cell. (**C′**,**C″**) The result of the clustering algorithm (C′) and the correlation map of the extent of axial coordination (C″) are shown. (**D**) Correlation map of the extent of axial coordination in the observed sample shown in Fig. 3D.

the orientation of cell division axes parallels the average direction of cell elongation (Fig. 5C). This reveals that cell divisions are oriented and follow the myofiber architecture of the fetal heart. In the embryonic heart (Fig. 5D), we first investigated the anisotropy of the distribution of the axes of cell division and showed that it follows a girdle distribution (Bingham and Giné's tests, P<0.001; Anderson-Stephens' test, Fig. 5E). To characterize the plane in which division axes lie preferentially, we measured the distribution of angles with the local transmural axis. The observed distribution significantly deviates from the random distribution (Fig. 5F), indicating that the axes of cell division in the embryonic heart tend to lie preferentially in a plane parallel to the outer surface of the heart. Within this plane, our clustering algorithm reveals a further local coordination of cell divisions (Fig. 5G). We found that the coordination of cell divisions was much more significant than that of the centrosome-nucleus axes (compare Fig. 3C with Fig. 5F). However, we have not detected any significant relationship between the orientation of the centrosome-nucleus axes and that of cell division axes. In some embryos, we observed a consistent pattern of the orientation of cell division: we drew the cumulative pattern (Fig. 5H), which indicates four regions of significant axial coordination in the left ventricle. As we had previously shown that growth of the myocardium is oriented (Meilhac et al., 2004a), we asked whether the orientation of cell clones parallels that of cell divisions. The map of clone orientation (Fig. 5I) is indeed very similar to that of the orientation of cell division.

The myocardium does not only grow in the plane of the heart surface, it also thickens transmurally, which leads to the formation of trabeculations. To find out whether the orientation of cell division also underlies trabecular growth, we investigated whether it varies along the transmural axis, by distinguishing cells on the surface from cells deeper within the myocardium (Fig. 6). Very rare cells have a division that parallels the trabeculations (Fig. 6B), whereas most cells, deeper or on the surface, tend to divide parallel to the heart surface (Fig. 6A,C).

Taken together, our data reveal that cell division is oriented in the developing heart, with a planar bias, and, at fetal stages, follows the myofiber architecture.

DISCUSSION

We provide a novel methodology for 3D analysis of tissue anisotropy. Our complete and sensitive procedure aims to characterize the anisotropy and alignment of a set of axes or vectors in a 3D tissue. We show that statistical tests of 3D axial distribution, which can distinguish between isotropic, bipolar and girdle distributions, reveal tissue anisotropy. Local average maps of orientations, which are commonly used, give only a poor description of the distribution. By contrast, our clustering algorithm

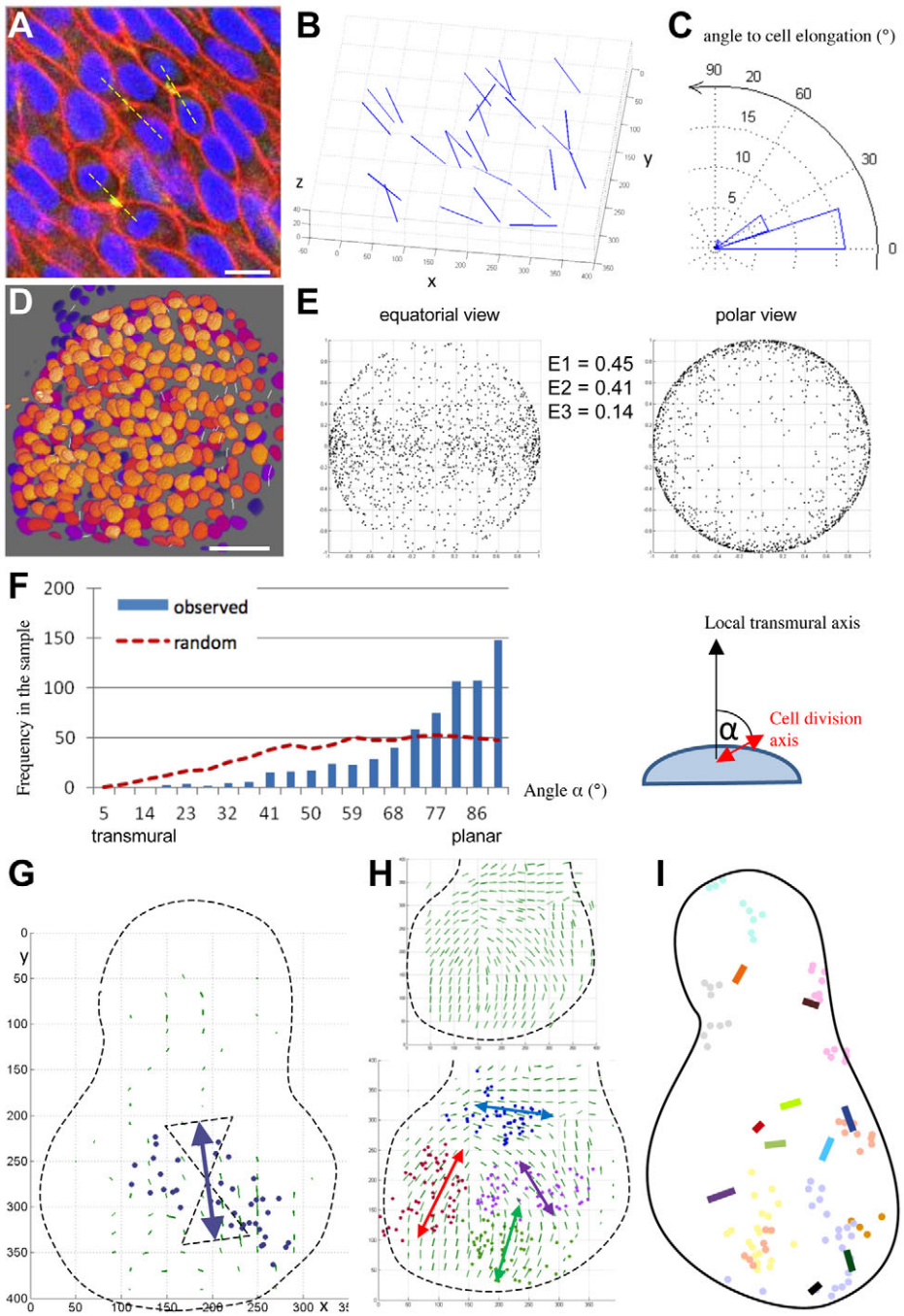

Fig. 5. Local coordination of cell divisions in fetal and embryonic hearts. (**A**) Example of an image of cells in the fetal heart, with labeled nuclei (blue), membranes (red) and cytoplasmic bridges (green). Dashed yellow lines join sister nuclei and indicate the orientation of cell division. Scale bar: 10 μm. (**B**) Map of the orientation of cell division in the ventricle of the fetal heart, in the same sample as in Fig. 2. Each axis (blue) gives the position and orientation of a cell division. (**C**) Rose diagram (five bins) of the angles between each axis of cell division and the average direction of cell elongation (significant Giné's test, $P<0.001$, $n=25$). (**D**) 3D view of segmented nuclei (brown) and cell division axes (white lines), taken from an embryonic heart. Scale bar: 50 μm. (**E**) The observed sample of axes of cell division significantly shows a non-isotropic girdle distribution (Anderson-Stephens' test, $P<0.01$, $n=682$ axes pooled from seven embryos). E, eigenvalue. (**F**) The distribution of the angles between the axes of cell division and the local transmural axis. The observed distribution was significantly different (Student's *t*-test, $P<0.001$, $n=682$) from a random spherical distribution and indicates a planar bias. (**G**) Map of the region (colored dots) with significant axial coordination around the average direction (double-headed arrow), with the corresponding s.d. (dotted line). The local average directions per box (green bars) are also shown. (**H**) Cumulative map of the regions (colored dots) in the left ventricle with significant axial coordination (regional directions shown by double-headed arrows), from the data of three different embryos. The local average directions per box (green bars) are also shown separately in the upper panel. (**I**) Schematic representation of an E8.5 heart, in the same view as in G, showing the orientation of clones of myocardial cells. Small clones of two cells (colored bars, $n=10$) and larger clones (pale dots, $n=7$ color-coded) are included.

provides a statistical assessment of the axis alignment compared with a random distribution. It results in an unbiased mapping of the regions with a significant axial coordination. Its power is shown by its sensitivity to detect weak anisotropies, such as the centrosome-nucleus axes in the embryonic heart. With the axial correlation function, the range of the local coordination of cells can be evaluated. We have validated our methodology on synthetic data, as well as for the fetal heart, in which tissue anisotropy is well characterized (Risebro et al., 2009).

By contrast, in the embryonic heart, tissue anisotropy had not been detected. We now show that the axes of cell polarity and of cell division lie preferentially in a plane parallel to the heart surface, with a minor transmural component. This is in agreement with different polarizing clues in the plane and the transmural axis. Planar signaling via the Wnt/PCP pathway has been shown to be essential for heart morphogenesis (Henderson and Chaudhry, 2011), although embryonic myocardial cells are not epithelial, with no evidence of apico-basal polarity (Hirschy et al., 2006). Alternatively, signals that control the transmural growth of the myocardium, are well characterized. For example, Notch signaling is active in the endocardium and is required for the transmural growth of the myocardium (Grego-Bessa et al., 2007).

Although PCP pathways are required for the growth of the myocardium, no asymmetric distribution of proteins has been described within the plane of cardiac chamber expansion and thus it had remained unclear how to monitor tissue polarity in the embryonic heart. We reveal that the centrosome-nucleus axes are

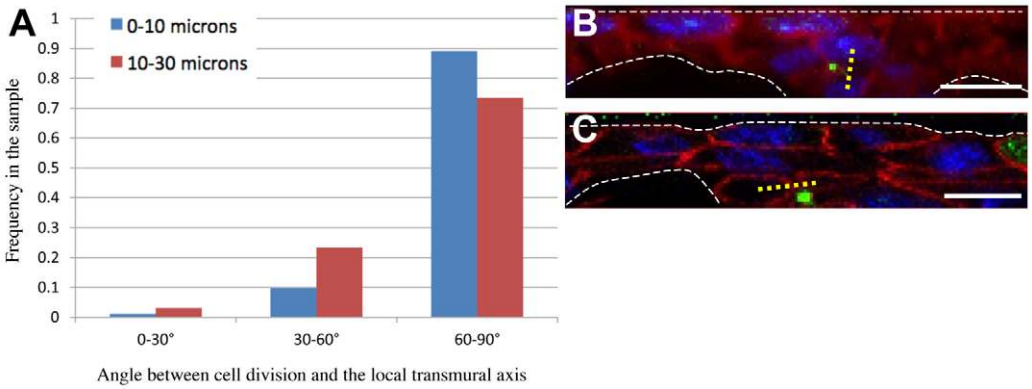

Fig. 6. Planar bias of cell divisions also in trabeculated myocardium. (**A**) Distribution of the angle between the axes of cell division and the local transmural axis, distinguishing surface (blue) or deeper (red) cells. (**B**) Example of a rare transmural division in a deeper cell. The cytoplasmic bridge (green) links the two sister nuclei (joined by a broken yellow line). The heart surface is at the top and the blood cavity at the bottom. (**C**) Example of a planar division in a deeper cell.

locally coordinated, before the myofiber architecture is apparent. In addition to the tissue architecture, we show that cell behavior is coordinated, as evidenced by oriented cell division. The orientation of cell division is more significantly coordinated than that of centrosome-nucleus axes. This may reflect the dynamics of centrosome positioning, e.g. during cell cycle progression. It also suggests that cell behavior is more tightly controlled than the position of the centrosome, as it is an integrated readout of different polarity signals (Morin and Bellaïche, 2011). In the embryonic heart, we have not detected a relationship between tissue architecture, as shown by the centrosome-nucleus axes, and the orientation of cell division. By contrast in the fetal heart, we found that the tissue architecture, as shown by the elongation of cells, parallels the orientation of cell division. In our previous clonal analysis, we had indeed detected different phases of tissue growth (Meilhac et al., 2003). A potential influence on tissue architecture and the orientation of cell division (Kada et al., 1999) is hemodynamics. Blood flow is a later determinant of heart shape and myofiber architecture (Granados-Riveron and Brook, 2012). However, during embryonic heart development, blood flow is progressively established (Nishii and Shibata, 2006), which would explain why the fetal heart is more organized. In mutants with an absence of heart contraction (Koushik et al., 2001), heart morphogenesis can proceed up to the looped heart tube, indicating that blood flow is dispensable for the early stages of myocardial growth.

We have previously shown, by clonal analysis, that the growth of the myocardium is regionally oriented and correlates with cardiac chamber expansion (Meilhac et al., 2004a), as well as with the myofiber architecture in the neonatal heart (Meilhac et al., 2003). Our results now suggest that the planar expansion of the myocardium may be mainly driven by oriented cell division, as division patterns are consistent with clonal patterns in the embryonic heart, and with the myofiber architecture in the fetal heart. In agreement with a minor role of cell intercalation, we also reported that growth of the myocardium is mainly coherent (Meilhac et al., 2003). By contrast, our results suggest that the transmural growth of trabeculations is not driven by oriented cell division, as we find that the orientation of cell division is not transmural, despite a general orientation of clones along the trabecular trajectory (Meilhac et al., 2003). Computer modeling will be required in order to understand how a combination of planar oriented cell division and a transmural gradient of cell proliferation (Sedmera et al., 2003) results in trabeculations.

The regions we have identified, with a significant cell coordination, do not obviously correlate with molecular or anatomical features, and rather reveal local polarizing processes. We have estimated that the range of the coordination extends over a number of cell diameters. In addition, the direction of cell coordination is maintained locally but shows regional variations. Although the molecular control of cell coordination remains to be elucidated, this pattern of coordination permits us to speculate on the mechanism of establishment of myocardial tissue polarity. Computer modeling has shown that tissue polarity, which is propagated at cell junctions, leads to local swirling patterns in the absence of a global polarizing signal (Burak and Shraiman, 2009). This corresponds to our observations in the embryonic heart, and is also consistent in the adult heart with the known architecture of the myofibers, which shows gradual variation and is described as a spiral around the ventricles (Jouk et al., 2000). The pattern of cell coordination that we demonstrate opens perspectives for the understanding of congenital heart diseases, in which myocardial architecture is frequently affected.

We provide a novel tool in biology that is applicable to other tissues in which 3D information is essential to address the mechanism of morphogenesis. It is applicable to mesenchyme, in which there is no obvious reference plane to perform a 2D analysis (Boehm et al., 2010), or to curved or branched epithelia, in which there is no simple reference axis (Matsuyama et al., 2009; Tang et al., 2011). We have applied this tool to several markers of polarity. It should also be useful for the quantification of the cellular differences between wild-type and mutant models with impaired polarity signaling. Thus, we anticipate that our methodology should contribute to the quantification of the behavior of systems, which is an emerging aspect of biology, as a pre-requisite to gain mechanistic insights into multiscale processes based on computer simulation (Sharpe, 2011).

Acknowledgements
We thank Y. Bellaïche, F. Graner and E. Coen for insightful comments on the manuscript. We thank F. de Chaumont for the wavelet-based spot detector.

Funding
The work was funded by the Institut Pasteur [PTR335 to S.M.], L'Agence Nationale de la Recherche [11-JSV2-00601 to S.M.], Le Centre National de la

Recherche Scientifique and Institut National de la Santé et de la Recherche Médicale. C.V.R. has benefited from a fellowship from the French Ministry of Research. J.F.L.G. was financed with grants from the EU Project 'CardioCell' [LT2009-223372 to M.E.B.] and from the Lefoulon-Delalande Foundation.

Competing interests statement
The authors declare no competing financial interests.

Supplementary material
Supplementary material available online at
http://dev.biologists.org/lookup/suppl/doi:10.1242/dev.087940/-/DC1

References

Anderson, T. W. and Stephens, M. A. (1972). Tests for randomness of directions against equatorial and bimodal alternatives. *Biometrika* **59**, 613-621.
Badano, J. L., Teslovich, T. M. and Katsanis, N. (2005). The centrosome in human genetic disease. *Nat. Rev. Genet.* **6**, 194-205.
Baena-López, L. A., Baonza, A. and García-Bellido, A. (2005). The orientation of cell divisions determines the shape of Drosophila organs. *Curr. Biol.* **15**, 1640-1644.
Blankenship, J. T., Backovic, S. T., Sanny, J. S. P., Weitz, O. and Zallen, J. A. (2006). Multicellular rosette formation links planar cell polarity to tissue morphogenesis. *Dev. Cell* **11**, 459-470.
Boehm, B., Westerberg, H., Lesnicar-Pucko, G., Raja, S., Rautschka, M., Cotterell, J., Swoger, J. and Sharpe, J. (2010). The role of spatially controlled cell proliferation in limb bud morphogenesis. *PLoS Biol.* **8**, e1000420.
Bornens, M. (2008). Organelle positioning and cell polarity. *Nat. Rev. Mol. Cell Biol.* **9**, 874-886.
Burak, Y. and Shraiman, B. I. (2009). Order and stochastic dynamics in Drosophila planar cell polarity. *PLoS Comput. Biol.* **5**, e1000628.
Cohen-Steiner, D., Alliez, P. and Desbrun, M. (2004). Variational shape approximation. *ACM Trans. Graph.* **23**, 905-914.
Concha, M. L. and Adams, R. J. (1998). Oriented cell divisions and cellular morphogenesis in the zebrafish gastrula and neurula: a time-lapse analysis. *Development* **125**, 983-994.
de Chaumont, F., Dallongeville, S., Chenouard, N., Hervé, N., Pop, S., Provoost, T., Meas-Yedid, V., Pankajakshan, P., Lecomte, T., Le Montagner, Y. et al. (2012). Icy: an open bioimage informatics platform for extended reproducible research. *Nat. Methods* **9**, 690-696.
Dufour, A., Thibeaux, R., Labruyère, E., Guillén, N. and Olivo-Marin, J. C. (2011). 3-D active meshes: fast discrete deformable models for cell tracking in 3-D time-lapse microscopy. *IEEE Trans. Image Process.* **20**, 1925-1937.
Efron, B. and Tibshirani, R. (1993). *An Introduction to the Bootstrap*. New York, NY: Chapman & Hall.
Gong, Y., Mo, C. and Fraser, S. E. (2004). Planar cell polarity signalling controls cell division orientation during zebrafish gastrulation. *Nature* **430**, 689-693.
Goodrich, L. V. and Strutt, D. (2011). Principles of planar polarity in animal development. *Development* **138**, 1877-1892.
Granados-Riveron, J. T. and Brook, J. D. (2012). The impact of mechanical forces in heart morphogenesis. *Circ. Cardiovasc. Genet.* **5**, 132-142.
Grego-Bessa, J., Luna-Zurita, L., del Monte, G., Bolós, V., Melgar, P., Arandilla, A., Garratt, A. N., Zang, H., Mukouyama, Y. S., Chen, H. et al. (2007). Notch signaling is essential for ventricular chamber development. *Dev. Cell* **12**, 415-429.
Gros, J., Hu, J. K.-H., Vinegoni, C., Feruglio, P. F., Weissleder, R. and Tabin, C. J. (2010). WNT5A/JNK and FGF/MAPK pathways regulate the cellular events shaping the vertebrate limb bud. *Curr. Biol.* **20**, 1993-2002.
Harvey, R. P. (2002). Patterning the vertebrate heart. *Nat. Rev. Genet.* **3**, 544-556.
Henderson, D. J. and Chaudhry, B. (2011). Getting to the heart of planar cell polarity signaling. *Birth Defects Res. A Clin. Mol. Teratol.* **91**, 460-467.
Hirschy, A., Schatzmann, F., Ehler, E. and Perriard, J. C. (2006). Establishment of cardiac cytoarchitecture in the developing mouse heart. *Dev. Biol.* **289**, 430-441.
Jouk, P. S., Usson, Y., Michalowicz, G. and Grossi, L. (2000). Three-dimensional cartography of the pattern of the myofibres in the second trimester fetal human heart. *Anat. Embryol. (Berl.)* **202**, 103-118.
Kada, K., Yasui, K., Naruse, K., Kamiya, K., Kodama, I. and Toyama, J. (1999). Orientation change of cardiocytes induced by cyclic stretch stimulation: time dependency and involvement of protein kinases. *J. Mol. Cell. Cardiol.* **31**, 247-259.
Koushik, S. V., Wang, J., Rogers, R., Moskophidis, D., Lambert, N. A., Creazzo, T. L. and Conway, S. J. (2001). Targeted inactivation of the sodium-calcium exchanger (Ncx1) results in the lack of a heartbeat and abnormal myofibrillar organization. *FASEB J.* **15**, 1209-1211.
Lecuit, T. and Lenne, P.-F. (2007). Cell surface mechanics and the control of cell shape, tissue patterns and morphogenesis. *Nat. Rev. Mol. Cell Biol.* **8**, 633-644.
Mardia, K. V. and Jupp, P. E. (2000). *Directional Statistics*. Chichester, UK: John Wiley & Sons.
Matsuyama, M., Aizawa, S. and Shimono, A. (2009). Sfrp controls apicobasal polarity and oriented cell division in developing gut epithelium. *PLoS Genet.* **5**, e1000427.
Meilhac, S. M., Kelly, R. G., Rocancourt, D., Eloy-Trinquet, S., Nicolas, J.-F. and Buckingham, M. E. (2003). A retrospective clonal analysis of the myocardium reveals two phases of clonal growth in the developing mouse heart. *Development* **130**, 3877-3889.
Meilhac, S. M., Esner, M., Kerszberg, M., Moss, J. E. and Buckingham, M. E. (2004a). Oriented clonal cell growth in the developing mouse myocardium underlies cardiac morphogenesis. *J. Cell Biol.* **164**, 97-109.
Meilhac, S. M., Esner, M., Kelly, R. G., Nicolas, J.-F. and Buckingham, M. E. (2004b). The clonal origin of myocardial cells in different regions of the embryonic mouse heart. *Dev. Cell* **6**, 685-698.
Morin, X. and Bellaïche, Y. (2011). Mitotic spindle orientation in asymmetric and symmetric cell divisions during animal development. *Dev. Cell* **21**, 102-119.
Muzumdar, M. D., Tasic, B., Miyamichi, K., Li, L. and Luo, L. (2007). A global double-fluorescent Cre reporter mouse. *Genesis* **45**, 593-605.
Nishii, K. and Shibata, Y. (2006). Mode and determination of the initial contraction stage in the mouse embryo heart. *Anat. Embryol. (Berl.)* **211**, 95-100.
Olivo-Marin, J. C. (2002). Extraction of spots in biological images using multiscale products. *Pattern Recognit.* **35**, 1989-1996.
Pop, S., Dufour, A. and Olivo-Marin, J. C. (2011a). Image filtering using anisotropic structure tensor for cell membrane enhancement in 3d microscopy. *Proceedings of 18th IEEE International Conference on Image Processing* 2041-2044.
Pop, S., Dufour, A., Le Garrec, J. F., Ragni, C. V., Buckingham, M. E., Meilhac, S. M. and Olivo-Marin, J. C. (2011b). A fast and automated framework for extraction of nuclei from cluttered 3D images in fluorescence microscopy. *Proceedings of IEEE International Symposium on Biomedical Imaging* 2113-2116.
Ringrose, T. J. and Benn, D. I. (1997). Confidence regions for fabric shape diagrams. *J. Struct. Geol.* **19**, 1527-1536.
Risebro, C. A., Searles, R. G., Melville, A. A. D., Ehler, E., Jina, N., Shah, S., Pallas, J., Hubank, M., Dillard, M., Harvey, N. L. et al. (2009). Prox1 maintains muscle structure and growth in the developing heart. *Development* **136**, 495-505.
Sedmera, D., Reckova, M., DeAlmeida, A., Coppen, S. R., Kubalak, S. W., Gourdie, R. G. and Thompson, R. P. (2003). Spatiotemporal pattern of commitment to slowed proliferation in the embryonic mouse heart indicates progressive differentiation of the cardiac conduction system. *Anat. Rec.* **274A**, 773-777.
Sepich, D. S., Usmani, M., Pawlicki, S. and Solnica-Krezel, L. (2011). Wnt/PCP signaling controls intracellular position of MTOCs during gastrulation convergence and extension movements. *Development* **138**, 543-552.
Sharpe, J. (2011). Two ways to use imaging: focusing directly on mechanism, or indirectly via behaviour? *Curr. Opin. Genet. Dev.* **21**, 523-529.
Strutt, D. I. (2001). Asymmetric localization of frizzled and the establishment of cell polarity in the Drosophila wing. *Mol. Cell* **7**, 367-375.
Tang, N., Marshall, W. F., McMahon, M., Metzger, R. J. and Martin, G. R. (2011). Control of mitotic spindle angle by the RAS-regulated ERK1/2 pathway determines lung tube shape. *Science* **333**, 342-345.
Wu, J. and Mlodzik, M. (2009). A quest for the mechanism regulating global planar cell polarity of tissues. *Trends Cell Biol.* **19**, 295-305.
Zallen, J. A. (2007). Planar polarity and tissue morphogenesis. *Cell* **129**, 1051-1063.